Stroeve, P.; Cervera, J.; Mafé, S.; Ramirez Hoyos, P. (2011). Asymmetric nanopore rectification for ion pumping, electrical power generation, and information processing applications. Electrochimica Acta. 56(12):4504-4511. doi:10.1016/j.electacta.2011.02.056.

Asymmetric nanopore rectification for ion pumping, electrical power generation, and information processing applications

Javier Cervera,[a] Patricio Ramirez,[b,*] Salvador Mafe,[a] and Pieter Stroeve[c]

[a]Departament de Física de la Terra i Termodinàmica, Universitat de València, E-46100 Burjassot, Spain

[b]Depto. de Física Aplicada, Universidad Politécnica de Valencia, E-46022 Valencia, Spain

[c]Department of Chemical Engineering, University of California Davis, Davis, CA 95616, USA

ABSTRACT

Single-track, asymmetric nanopores can currently be functionalised with a spatially inhomogeneous distribution of fixed charges and a variety of pore tip shapes. Optimising the asymmetric nanopore characteristics is crucial for practical applications in nanofluidics. We have addressed here this question for three cases based on different input/output chemical and electrical signals: (*i*) ion pumping up a concentration gradient by means of a periodic, time-dependent bias potential, (*ii*) information processing with a single nanopore acting as the nanofluidic diode of a logic gate, and (*iii*) electrical energy harvesting using a nanopore that separates two solutions of different salt concentrations. The results show the nanopore characteristics (size, shape, and charge distribution) that should be optimised for each application. In particular, the control of the pore tip size and charge appears to be crucial in all cases because it is in this narrow region where the interaction of the ions and the pore surface occurs, and this will eventually determine the nanodevice performance.

KEYWORDS: Ionic transport, synthetic nanopores

*Corresponding Author, E-mail: patraho@fis.upv.es

1. **Introduction**

Nanopores, nanopipettes, nanofluidic channels, and nanoelectrodes constitute a new generation of devices designed for single-molecule sensing and separation [1-15]. Nanostructures based on asymmetric pores with only one type of electric charge, bipolar diodes and transistors composed by regions of different charge juxtaposed in series, and nanofluidic diodes with amphoteric chains functionalised on the pore surface have been reported [15-20]. Most previous studies concern fundamental research on the nanostructure characteristics, with emphasis on the ionic selectivity and rectification properties [21-28]. These properties are usually based on the nanopore fixed charges and nanostructure asymmetry. However, practical applications will require both the design of applied schemes based on the nanostructure characteristics and the study of new experimental methods to tune the nanopore selectivity and conductance.

Single-track, asymmetric nanopores can currently be functionalised with spatially inhomogeneous distributions of fixed charges and a variety of pore tip shapes [17, 29-32]. Optimizing the asymmetric nanopore characteristics is crucial for nanofluidics applications. We have addressed here this question for three cases based on different input/output chemical and electrical signals: (*i*) ion pumping up a concentration gradient using a periodic, time-dependent bias potential [1, 33], (*ii*) information processing with a single nanopore acting as the nanofluidic diode of a logic gate [34], and (*iii*) electrical energy harvesting by means of a nanopore that separates two solutions of different salt concentrations [35]. This study is timely because it has recently become possible for the reproducible fabrication of nanostructures with pre-determined geometries and controlled structural asymmetries [13, 15, 29, 31, 36]. In particular, the control of the shape and size opens the possibility to design and construct nanopores aimed at performing a specific function efficiently. Note also that single pores may constitute elementary building blocks for nanoporous membranes, and the

understanding and control of their individual properties is a previous step for designing membranes with improved efficiency in protein separation, water desalination, and bio-molecule detection using arrays of identical nanopores [7, 10, 13, 37-39].

Most studies with nanometer-scaled pores concern molecular separation and sensing applications [2, 5, 7-11, 37, 40]. However, ion pumping between two solutions up a concentration gradient, information processing based on different nanopore conductance levels, and electrical energy generation with two solutions at different salt concentrations are also significant problems for both biological ion channels [41] and membrane chemical engineering [13, 34, 35, 42]. In particular, implementing these processes in practical devices will demand: (*i*) a better knowledge of the physical conditions dictating ion pumping (the relationship between the asymmetric nanostructure characteristics and the applied periodic potential should be clarified), (*ii*) a significant improvement of the nanopore rectification properties, and (*iii*) a clear understanding of the nanopore characteristics entering in the electrical circuit used for the conversion of chemical energy into electrical energy. While previous theoretical calculations based on continuum model equations have shown how the distribution of fixed charges [25, 31, 43] and the pore tip shape [20, 26, 44] dictate the rectification properties, thorough studies aimed at improving the nanopore performance for practical applications are still lacking. We have addressed this question here, obtaining predictions of conceptual interest for efficient application of the broad list of chemically and electrochemically switchable nanopores reported [2, 9, 10, 16-19, 34, 37, 40, 45-49].

2. Model equations

The nanopore and transport equations modelling will be guided by recent studies on nanopore fabrication showing typical tip shapes and dimensions [20, 44] as well as by previous experimental characterisations of the selectivity and rectification properties in nanopores [17, 19-23, 26, 34, 44]. Fig. 1 illustrates schematically the fabrication procedure of

the nanopore by track-etching. First, a polymer foil is irradiated with heavy ions (e.g., Xe, Pb, U and Au) of high energy. The number of ions passing through the foil gives the number of latent tracks formed in the polymer sample. By limiting the number of impinging ions, it is possible to obtain samples with only one track [50, 51] (Fig. 1A). Second, the latent tracks are etched with alkali and converted into nanopores whose size and shape can be tailored by controlling the temperature and duration of etching, using specific surfactants, and exposing the foil surfaces to ultraviolet radiation. This procedure allows for the fabrication of nanopores with a variety of symmetric and asymmetric longitudinal shapes (e.g., cylindrical [52], conical [51], double conical [18], concave pores with bullet-like tips [30, 53], and convex pores with trumpet-like tips [29]).

The process of etching with alkali results in the formation of carboxylate groups (COO^-) on the inner pore surface [51]. In the recent years, different techniques allowing for efficient control of a variety of fixed charge groups attached on the pore wall have been developed [17-20, 29, 31, 34, 38, 54-57]. Because of the high number of pores with different longitudinal shapes and fixed charge distributions, we have limited our study to the characteristic cases of concave, bullet-like tip, and conical pores with negative fixed charges homogeneously distributed over the pore surface, as well as to conical pores where the negative fixed charge is confined to the region of the pore tip (Fig. 1B). These geometries cover most of the experimental designs [17, 20, 25, 27, 29-31, 53, 58]. To describe this variety of pore shapes and sizes, we introduce the following exponential profile for the nanopore radius $a(x)$

$$a(x) = \frac{a_R - a_L \exp(-d/h) - (a_R - a_L)\exp\left[-(x/d)(d/h)\right]}{1-\exp(-d/h)}\,, \tag{1}$$

where a_L and a_R are the radii at the tip and base of the pore, respectively, and d is the pore length. Parameter d/h controls the shape of the pore: the limit $d/h \to 0$ gives a conical pore while increasing d/h enlarges the lumen region (the pore gets more tapered; see Fig. 1C, left).

Regarding the surface charge distribution along the pore axis, we assume that the density of fixed charges varies with coordinate x according to the following step-like function

$$\sigma(x) = \sigma_0 \left[-1 + \frac{1}{1 + \exp\left[-2k\left(x - x_0 \right) \right]} \right], \tag{2}$$

where σ_0 gives the surface charge concentration in the limit $x \to 0$, x_0 is the position at the pore axis where $\sigma(x_0) = \sigma_0/2$, and parameter k is defined as

$$k = -\frac{1}{w} \log\left[\tanh\left(\frac{1}{2} \right) \right], \tag{3}$$

where the characteristic length w (Fig. 1C, right) is a measure of the thickness of the transition zone located between $\sigma \approx \sigma_0$ (for $x << x_0$) and $\sigma \approx 0$ (for $x >> x_0$).

The length of the pores considered in this study is d = 12 μm. The pore radii vary from some hundreds of nanometres at the wide base to less than 10 nm at the narrow tip [13]. In all the cases we have assumed a_L = 5 nm and a_R = 300 nm. Using these characteristics values [13] consistently throughout the study allows comparing the results obtained for the different geometries.

The basic equations describing the ionic transport through the nanopore are the Nernst-Planck equations [59]

$$\vec{J}_i = -D_i \left(\nabla c_i + z_i c_i \frac{F}{RT} \nabla \phi \right), \tag{4}$$

the Poisson equation

$$\nabla^2 \phi = -\frac{F}{\varepsilon} \sum_i z_i c_i \,, \tag{5}$$

and the continuity equation

$$\nabla \cdot \vec{J}_i = 0\,, \tag{6}$$

where $\vec{J}_i$, D_i and z_i are the ionic flux density, the diffusion coefficient and the charge number of ion i; F and R are the Faraday and universal gas constants, and T is the absolute temperature; ϕ and ε are the local electric potential and the electrical permittivity of the solution within the pore. Throughout this paper, positive bias potentials are applied on the solution facing the narrow opening, and positive currents flow from the narrow towards the wide opening of the nanopore. Numerical integration of equations (4)-(6) gives the ionic concentration and potential profiles, the ionic flux densities, and the current I passing through any arbitrary section of the nanopore at any applied potential difference ΔV. To this end, different numerical procedures can be used [21-26, 44]. In the case of the pore geometries considered in this paper, the problem can be simplified significantly. Because the pore is long and narrow, the ionic flux densities can be assumed to have only the axial component. Also, in the case of long pores, the electroneutrality condition can be used instead of the Poisson equation, and the influence of the access resistance can be neglected, assuming then Donnan equilibrium at the nanopore/solution interfaces. Following this procedure, the original 2D geometry can be reduced to a 1D problem, and the resulting two-point boundary value problem can be efficiently solved using iterative schemes such as the shooting or the relaxation methods (see reference [44] for further details).

Note that the electrical interactions between the nanopore fixed charges and the mobile charges in the inside solution can be described by continuum models (the Poisson and Nernst-Planck (PNP) equations are used here) whose validity have been previously confirmed [19, 22-25, 44, 46]. They are valid for pores with relatively wide openings and moderate fixed surface charge concentrations like the ones considered here. In these cases, the pore radii are larger than the Debye screening length over most of the experimental concentration range

and, in turn, these radii are much greater than the ion size [60-62]. Recent molecular dynamics (MD) simulations on the ionic current passing through charged cylindrical nanopores [62] reveal that the discrepancies between the electric currents calculated using the MD and PNP approaches can be higher than 10% only in the case of pores with radii of the order of 1 nm and surface fixed charge concentrations higher than -1.2 e/nm^2, where e is the elementary charge.

3. Results and discussion

Fig. 2 shows the current-applied potential difference (I-ΔV) and rectification ratio-applied potential difference (r-ΔV) curves of asymmetric nanopores (the rectification ratio is defined as $r = |I(\Delta V)/I(-\Delta V)|$). We have considered nanopores with bullet-like pore tip and fixed charges homogeneously distributed on the pore surface (Fig. 2A) as well as conical pores where the fixed charges are confined to the region of the pore tip (Fig. 2B). In all cases, we consider the typical surface charge density $\sigma_0 =$ -1 e/nm^2 [19, 21, 22, 25, 26, 34]. The results in Fig. 2A are parametric in d/h (the conical nanopore corresponds to the limit $d/h \rightarrow 0$). The curves in Fig. 2B are parametric in the thickness x_0 of the charged region, with w = 2 nm in Eq. (3) (the case of the conical pore is shown again for the sake of comparison). The results emphasise the nanopore characteristics (pore tip shape and thickness of the charge distribution) needed to modulate efficiently the conductance and rectification properties. The basic rectification properties of Fig. 2 have been confirmed both theoretically and experimentally [19, 20, 22, 24-28, 31, 34, 61] and will allow understanding the results in Figs. 3-5 later. The origin of the rectification phenomenon has been discussed in detail previously [21-26, 44]. The electric potential profiles are strongly nonlinear in the region of the pore tip, where the effects of the fixed charges are more noticeable. At a given value $\Delta V > 0$, the electric field drags the majority ions to the pore tip, where these ions tend to accumulate due

to the fixed charges, and this leads to high pore conductance values. For $\Delta V < 0$, however, the electric field drives the majority ions out of the narrow pore region and the pore conductance attains values lower than those found for $\Delta V > 0$. The *I*- ΔV curves of Fig. 2A (left) show that *I* increases rapidly with *d*/*h* at a given $\Delta V > 0$. On the contrary, |*I*| hardly depends on *d*/*h* for $\Delta V < 0$. The results show then a rapid increase of *r* with *d*/*h* (Fig. 2A, right). In the case of the *I*- ΔV curves of Fig. 2B (left), the higher relative changes of |*I*| with x_0 occur now for $\Delta V < 0$. Figs. 2A and 2B (right) show that a significant increase of *r* (with respect to the case of the conical pore) can be achieved by controlling the pore shape and charge distribution while keeping constant the pore openings.

Figs. 3A-C show the principles of ion pumping using asymmetric nanopores. A polymeric film containing a single nanopore separates two KCl solutions of concentrations c_L (left solution facing the pore tip) and c_R (right solution facing the wide opening). For $c_L < c_R$ and no applied potential difference, there is a diffusive flow of potassium ions from the wide opening towards the tip of the pore (A). In this case, there is a potential gradient (the so called the reversal potential) that permits to estimate the nanopore selectivity via the ionic transport numbers, and this allows a deeper characterization of the basic mechanisms involved in ionic transport [23] (A complete theoretical and experimental study of the reversal potential in nanopores can be found in [23].) When a periodic input applied potential difference $\Delta V_{in}(t)$ of zero time average is applied (C), the time average output current $\langle I_{out}(t) \rangle$ is nonzero because of the rectification characteristics of the asymmetric nanopore (B). Fig. 3D shows $\langle I_{out}(t) \rangle$ as a function of the amplitude of the applied potential difference. Positive values correspond to uphill transport (transport against the concentration gradient). Note that for amplitudes of the applied potential difference lower than the threshold value ΔV_p, the imposed electrical driving force can not overcome the concentration gradient, and the average current is still negative

(downhill transport, see Figs. 3A and D). Fig. 3D shows also that when the concentration difference becomes larger, the ion pumping effect diminishes, and the threshold value ΔV_p shifts to higher values.

Figs. 3E and F show ΔV_p as a function of the concentration ratio c_R/c_L for the cases of a completely charged conical pore, a pore with bullet-like tip (d/h = 20), and a conical pore partially charged (x_0 =20 nm and w = 2 nm). The partially charged pore shows threshold values consistently lower than the other pores, being more efficient for ion pumping applications. This is in agreement with the rectification ratio values of Figs. 2A and 2B (right).

Most studies with nanometer-scaled pores concern molecular separation and sensing applications [2, 5, 7-11, 13, 37, 40], but not logic devices despite the fact that biological ion channels with *pH*-dependent fixed charges are known to be responsible for information processing in biophysical structures [41]. We have demonstrated theoretically and experimentally that single-track conical nanopores functionalised with polyprotic acid chains show three levels of conductance that can be tuned externally (because of the *pH*-sensitive fixed charges) and proposed a logic gate scheme where binary and multivalued logical functions were implemented using chemical and electrical inputs [34]. (Other recent proposals for logical gates involving chemical concepts can be found in Refs. [63-67].) Integration of microchannels and nanopores in chip-based ionic circuits [66, 67] should allow fast system responses in analytical applications involving information processing with logic circuits.

Fig. 4 shows the operating schemes for the *OR* logic gate A and the *I*-ΔV characteristics of the asymmetric nanopores B, which are those of Fig. 3. The size of the arrows constitutes a measure of the expected currents and the numbers correspond to the logic values assigned to the input and output applied potentials. Fig. 4B shows that at high positive ΔV values the nanopore is in the high-conducting state while at negative ΔV values the

opposite case occurs. The applied potentials V_i (i = 1,2) in the truth tables of Fig. 4B are the inputs and the potential V_{out} at the load resistance R = 100 MΩ is the output. Logic inputs (outputs) "1" and "0" correspond with high and low values of V_i (V_{out}), respectively. In each case, the output potential V_{out} is obtained by solving the electrical circuit with the input values of the respective nanopore resistances and a logical output (the value between parentheses) is then assigned. $|V_{out}/V_{out,min}|$ (last column) corresponds to the ratio of the output potentials obtained in each particular case to the minimum potential (output "0"), which constitutes a measure of the efficiency of the logical gate based on the nanopore.

The bullet-like tip and the partially charged pores show significantly better performances than the conical pore. Again, it is the partially charged pore the most suitable one to implement the logical function because of its high rectification ratio. Indeed, the values of $|V_{out}/V_{out,min}|$ for the partially charged pore are a factor 10 higher than those obtained with the homogeneously charged conical pore. We emphasise that this significant increase in the nanopore efficiency is achieved just by a judicious choice of the charge distribution along the pore. Other nanofluidic architectures could now be used to implement a complete logic gate scheme [34] on the basis of the tuning of the nanopore conductance.

Recently, nanopores have been proposed as basic units for energy-harvesting using pressure and chemical concentration gradients [35, 68]. In particular, the efficiency of the power generation based on a salinity-gradient should be optimised by appropriate tailoring of the surface charge distribution and nanopore geometry. We have considered this problem in Figs. 5A-E for the asymmetric nanopores used here. The nanopore separates now two electrolyte solutions at different concentrations and displays the I-ΔV curve of Figs. 5A and B. When connected to an external load resistance, the nanopore and the solutions behave as a power source, as shown schematically in Fig. 5C (see Ref. [35] for details). The electrical

magnitudes of the Thèvenin equivalent circuit of Fig. 5C are the open circuit potential difference ΔV_{oc} and the zero-volt current I_0 defined in Figs. 5A and B [35].

Fig. 5D shows the values of ΔV_{oc} (left), $|I_0|$ (center), and $P_0 = \Delta V_{oc}\,|I_0|$ (right), which is proportional to the maximum power that can be achieved by connexion to an external load, as a function of c_R for the typical concentrations c_L = 0.1 mol dm^{-3} and 0.01 mol dm^{-3}. The asymmetric nanopores are those of Figs. 3 and 4. The partially charged nanopore shows values of ΔV_{oc} and $|I_0|$ significantly lower than the other two nanopores. Indeed, because the power generation is based on the experimental currents obtained rather than on the rectification efficiency, the bullet-like pore is now the best choice (see Fig. 2). When we compare the results of Fig. 5 with those of Figs. 3 and 4, it is concluded that the nanopore characteristics (size, shape, and charge distribution) that should be optimised for each particular application may be different, though the control of the pore tip appears to be crucial in all cases. It is in this narrow region where the interaction of the ions and the pore surface occurs, and this will eventually determine the device performance. The characteristics of the tip region can be tuned by both the fixed charge distribution and the tip shape. Interestingly, the charge distribution can also be modified chemically (e.g. by changing the solution *pH* and temperature, or adding divalent cations) without changing the nanopore structural characteristics dictated by the fabrication processes [19, 32, 34, 55, 69].

4. Conclusions

In conclusion, we have described how asymmetric nanopores can be functionalised with spatially inhomogeneous distributions of fixed charges and different pore tip shapes to optimize those characteristics essential for different practical applications with chemical and electrical signals as input/output values. These applications are: (*i*) ion pumping against a concentration gradient by means of a periodic, time-dependent applied potential difference,

(*ii*) information processing with nanopores acting as the nanofluidic diodes of a logic gate, and (*iii*) electrical energy harvesting using a nanopore that separates two solutions of different salt concentrations. The results show clearly that there are clues experimentally available that can be exploited to improve the nanopore performance for each application. In particular, the effective length of the narrow tip can be tuned by the fixed charge distribution and shape.

Acknowledgments

We acknowledge the financial support from the Ministry of Science and Innovation of Spain and *FEDER*, Programme of Materials (project No. *MAT2009-07747*).

Figure captions

Figure 1

Fabrication procedure of the nanopore by track-etching (A). The characteristic geometries of concave, bullet-like tip, and conical pores with negative fixed charges (B). Spatial parameters controlling the pore shape and charge distribution (C). *h* is a parameter whose relative value compared with the pore thickness *d* controls the pore shape: increasing *d*/*h* enlarges the lumen region and the pore becomes more tapered (Fig. 1C, left). *w* is a parameter that gives the thickness of the transition region where the fixed charge concentration decreases from $\sigma \approx \sigma_0$ for $x << x_0$ to $\sigma \approx 0$ for $x >> x_0$ (Fig. 1C, right).

Figure 2

Current-applied potential difference (*I*-Δ*V*) and rectification ratio- applied potential difference (*r*-Δ*V*) curves of asymmetric nanopores for a bullet-like pore tip with fixed charges homogeneously distributed (A) and a conical pore with fixed charges confined to the tip (B). The results in Fig. 2(A) are parametric in *d*/*h* while those of Fig. 2(B) are parametric in the thickness x_0 of the charged region.

Figure 3

Principles of ion pumping using asymmetric nanopores (A-C). A polymeric film contains a single nanopore that separates two KCl solutions of concentrations c_L and c_R (A). When a periodic input applied potential difference $\Delta V_{in}(t)$ of zero time average is applied (C), the time average output current $\langle I_{out}(t) \rangle$ is nonzero (B). $\langle I_{out}(t) \rangle$ as a function of the amplitude of the input applied potential difference. Positive values correspond to uphill transport (transport

against the concentration gradient) and occur only above the threshold value ΔV_p (D). ΔV_p as a function of the concentration ratio c_R/c_L for different pore geometries and salt concentrations (E,F).

Figure 4

Operating schemes for the *OR* logic gate. The size of the arrows is a measure of the expected currents and the numbers correspond to the logic values assigned to the input and output applied potentials (a). The *I*-Δ*V* characteristics of the asymmetric nanopores and the truth tables of the logic function implemented with the nanopore. The applied potentials V_i (i = 1,2) in the truth tables are the inputs and the potential V_{out} at the load resistance R = 100 MΩ is the output. Logic inputs (outputs) "1" and "0" correspond with high and low values of V_i (V_{out}) (B).

Figure 5

Energy harvesting using an asymmetric nanopore, which separates two electrolyte solutions at different concentrations, and the *I*-Δ*V* curve (A and B). Scheme of the power source with the electrical magnitudes of the Thèvenin equivalent circuit (C). Open circuit potential difference ΔV_{oc} (left), zero-volt current $|I_0|$ (center), and power $P_0 = V_{oc}\,|I_0|$ (right) as a function of c_R for the concentrations c_L = 0.1 mol dm^{-3} and 0.01 mol dm^{-3} (d).

References

[1] Z. Siwy, A. Fulinski, Phys. Rev. Lett. 89 (2002) 198103.

[2] S. Lee, Y. H. Zhang, H. S. White, C. C. Harrell, C. R. Martin, Anal. Chem. 76 (2004) 6108.

[3] K. Lebedev, S. Mafe, P. Stroeve, J. Phys. Chem. B 109 (2005) 14523.

[4] Y. H. Zhang, B. Zhang, H. S. White, J. Phys. Chem. B 110 (2006) 1768.

[5] S. Umehara, N. Pourmand, C. D. Webb, R. W. Davis, K. Yasuda, M. Karhanek, Nano Lett. 6 (2006) 2486.

[6] C. Dekker, Nature Nanotechnology 2 (2007) 209.

[7] J. R. Ku, S. M. Lai, N. Ileri, P. Ramirez, S. Mafe, P. Stroeve, J. Phys. Chem. C 111 (2007) 2965.

[8] R. W. Murray, Chem. Rev. 108 (2008) 2688.

[9] M. Ali, B. Yameen, R. Neumann, W. Ensinger, W. Knoll, O. Azzaroni, J. Am. Chem. Soc. 130 (2008) 16351.

[10] K. Healy, B. Schiedt, A. P. Morrison, Nanomedicine 2 (2007) 875.

[11] S. Umehara, M. Karhanek, R. W. Davis, N. Pourmand, Proc. Natl. Acad. Sci. U.S.A. 106 (2009) 4611.

[12] R. Yan, W. Liang, R. Fan, P. Yang, Nano Lett. 9 (2009) 3820.

[13] Z. S. Siwy, S. Howorka, Chem. Soc. Rev. 39 (2010) 1115.

[14] J. M. Perry, K. Zhou, Z. D. Harms, S. C. Jacobson, ACS Nano 4 (2010) 3897.

[15] L.-X. Zhang, X.-H. Cao, Y.-B. Zheng, Y.-Q. Li, Electrochem. Comm. 12 (2010) 1249.

[16] Z. Siwy, E. Heins, C. C. Harrell, P. Kohli, C. R. Martin, J. Am. Chem. Soc. 126 (2004) 10850.

[17] I. Vlassiouk, Z. Siwy, Nano Lett. 7 (2007) 552.

[18] E. B. Kalman, I. Vlassiouk, Z. Siwy, Adv. Mater. 20 (2008), 293.

[19] M. Ali, P. Ramirez, S. Mafe, R. Neumann, W. Ensinger, ACS Nano 3 (2009) 603.

[20] M. Ali, B. Yameen, J. Cervera, P. Ramirez, R. Neumann, W. Ensinger, W. Knoll, O. Azzaroni, J. Am. Chem. Soc. 132 (2010), 8338.

[21] J. Cervera, B. Schiedt, P. Ramirez, Europhys.Lett. 71 (2005) 35.

[22] J. Cervera, B. Schiedt, R. Neumann, S. Mafe, P. Ramirez, J. Chem. Phys. 124 (2006) 104706.

[23] J. Cervera, A. Alcaraz, B. Schiedt, R. Neumann, P. Ramirez, J. Phys. Chem. C 111, (2007) 12265.

[24] D. Constantin, Z. S. Siwy, Phys. Rev. E 76 (2007) 041202.

[25] X. Wang, J. Xue, L. Wang, W. Guo, W. Zhang, Y. Wang, Q. Liu, H. Ji, Q. Ouyang, J. Phys. D: Appl. Phys. 40 (2007) 7077.

[26] Q. Liu, Y. Wang, W. Guo, H. Ji, J. Xue, Q. Ouyang, Phys. Rev. E 75 (2007) 051201.

[27] A. Radenovic, E. Trepagnier, R. Csencsits, K. H. Downing, J. Liphardt, Appl. Phys. Lett. 93 (2008) 183101.

[28] M. L. Kovarik, K. Zhou, S. C. Jacobson, J. Phys. Chem. B 113 (2009) 15960.

[29] C. C. Harrell, Z. S. Siwy, C. R. Martin, Small 2 (2006) 194.

[30] P. Y. Apel, I. V. Blonskaya, S. N. Dmitriev, O. L. Orelovitch, A. Presz, B. A. Sartowska, Nanotechnology 18 (2007) 305302.

[31] M. Davenport, A. Rodriguez, K. J. Shea, Z. S. Siwy, Nano Lett. 9 (2009) 2125.

[32] X. Hou, Y. Liu, H. Dong, F. Yang, L. Li, L. Jiang, Adv. Mater. 22 (2010) 2440.

[33] Z. Siwy, A. Fulinski, Am. J. Phys. 72 (2004) 567.

[34] M. Ali, S. Mafe, P. Ramirez, R. Neumann, W. Ensinger, Langmuir 25 (2009) 11993.

[35] W. Guo, L. Cao, J. Xia, F.-Q. Nie, W. Ma, J. Xue, Y. Song, D. Zhu, Y. Wang, L. Jiang, Adv. Funct. Mat. 20 (2010) 1339.

[36] X. P. A. Gao, Zheng, G.; Lieber, C. M. Nano Lett. 10 (2010) 547.

[37] K.-Y. Chun, S. Mafe, P. Ramirez, P. Stroeve, Chem. Phys. Lett. 418 (2006) 561.

[38] Z. Siwy, L. Trofin, P. Kohli, L. A. Baker, C. Trautmann, C. R. Martin, J. Am. Chem. Soc. 127 (2005) 5000.

[39] R. B. Schoch, J. Han, P. Renaud, Rev. Mod. Phys. 80 (2008), 839.

[40] L.-J. Cheng, L. J. Guo, ACS Nano 3 (2009) 575.

[41] B. Hille, Ion channels of excitable membranes; Sinauer Associates: Sunderland, MA, (2001).

[42] P. Ramirez, A. Alcaraz, S. Mafe, J. Membrane Sci. 135 (1997) 135-144.

[43] P. Ramirez, V. Gomez, J. Cervera, B. Schiedt, S. Mafe, J. Chem. Phys. 126 (2007) 194703.

[44] P. Ramirez, P. Y. Apel, J. Cervera, S. Mafe, Nanotechnology 19 (2008) 315707.

[45] R. Fan, M. Yue, R. Karnik, A. Majumdar, P. Yang, Phys. Rev. Lett. 95 (2005) 086607.

[46] R. Karnik, R. Fan, M. Yue, D. Li, P. Yang, A. Majumdar, Nano Lett. 5 (2005) 943.

[47] S. W. Nam, M. J. Rooks, K. B. Kim, S. M. Rossnagel, Nano Lett. 9 (2009) 2044.

[48] E. B. Kalman, O. Sudre, I. Vlassiouk, Z. Siwy, Anal. Bioanal. Chem. 394 (2009) 413.

[49] P. Joshi, A. Smolyanitsky, L. Petrossian, M. Goryll, M. Saraniti, T. J. Thornton, J. Appl. Phys. 107 (2010) 054701.

[50] Y. E. Korchev, C. L. Bashford, G.M. Alder, P. Y. Apel, D. T. Edmonds, A. A. Lev, K. Nandi, A. V. Zima, C. A. Pasternak, FASEB J. 11 (1997) 600.

[51] Z. Siwy, Y. Gu, H. A. Spohr, D. Baur, A. Wolf-Reber, R. Spohr, P. Apel, Y. E. Korchev, Europhys. Lett. 60 (2002) 349.

[52] A. A. Lev, Y. E. Korchev, T. K. Rostovtseva, C. L. Bashford, D. T. Edmonds, C. A. Pasternak, Proc. R. Soc. London, Ser. B 252 (1993) 187.

[53] O. L. Orelovich, B. A. Sartowska, A. Presz, P. Y. Apel, J. Microsc. 237 Pt 3 (2010) 404.

[54] M. Ali, B. Schiedt, K. Healy, R. Neumann, W. Ensinger, Nanotechnology 19 (2008) 085713.

[55] Y. He, D. Gillespie, D. Boda, I. Vlassiouk, R. S. Eisenberg, Z. S. Siwy, J. Am. Chem. Soc. 131 (2009) 5194.

[56] X. Hou, W. Guo, F. Xia, F.-Q. Nie, H. Dong, Y. Tian, L. Wen, L. Wang, L. Cao, Y. Yang, J. Xue, Y. Song, Y. Wang, D. Liu, L. Jiang, J. Am. Chem. Soc. 131 (2009) 7800.

[57] B. Yameen, M. Ali, R. Neumann, W. Ensinger, W. Knoll, O. Azzaroni, Nano Lett. 9 (2009) 2788.

[58] R. Spohr, C. Zet, B. E. Fischer, H. Kiesewetter, P. Apel, I. Gunko, T. Ohgai, L. Westerberg, Nucl. Instrum. Methods Phys. Res. Sect. B 268 (2010) 676.

[59] K. Kontturi, L. Murtomäki, J. A. Manzanares, Ionic Transport Processes, Oxford University Press: Oxford, UK (2008).

[60] J. Cervera, P. Ramirez, J. A. Manzanares, S. Mafe, Microfluid Nanofluid 9 (2010) 41.

[61] Y. Ai, M. Zhang, S. W. Joo, M. A. Cheney, S. Qian, J. Phys. Chem. C 114 (2010) 3883.

[62] J. M. Xue, X. Q. Zou, Y. B. Xie, Y. G. Wang, J. Phys. D: Appl. Phys. 42 (2009) 105308.

[63] M. Pita, M. Krämer, J. Zhou, A. Poghossian, M. J. Schöning, V. M. Fernandez, E. Katz, ACS Nano 2 (2008) 2160.

[64] R. Ferreira, P. Remon, U. Pischel, J. Phys. Chem. C 113 (2009) 5805.

[65] J. Cervera, S. Mafé, Chem. Phys. Chem. 11 (2010) 1654.

[66] J.-H. Han, K. B. Kim, H. C. Kim, T. D. Chung, Angew. Chem. Int. Ed. 48 (2009) 3830.

[67] W. Zhan R. M. Crooks, J. Am. Chem. Soc. 125 (2003) 9934.

[68] Y. B. Xie, X. Wang, J. Xue, K. Jin, L. Chen, Y. Wang, Appl. Phys. Lett. 93 (2008) 163116.

[69] B. Yameen, M. Ali, R. Neumann, R. Ensinger, W. Knoll, O. Azzaroni, Small 5 (2009) 1287.

Asymmetric nanopores obtained by track-etching

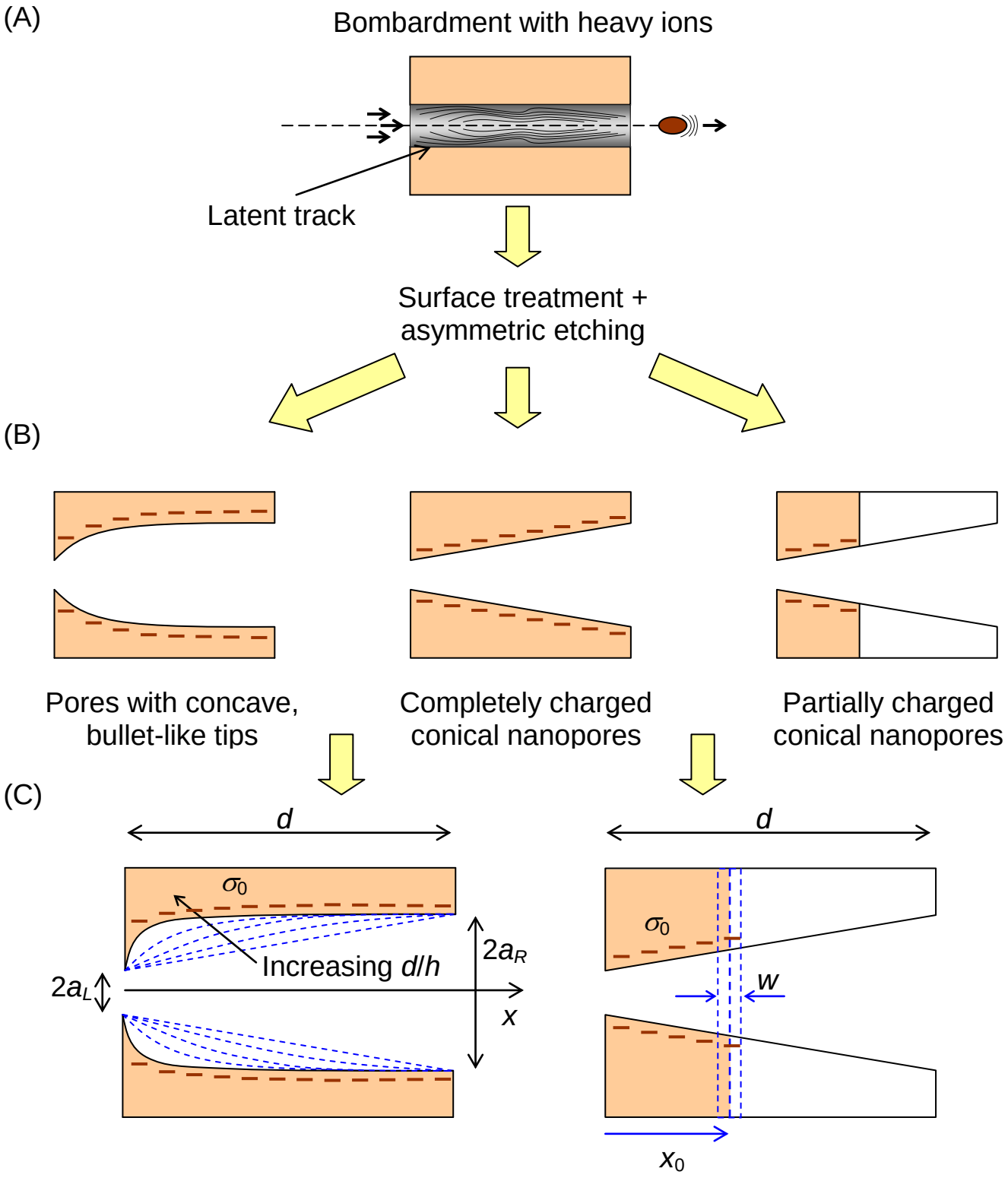

Figure 1

Current – applied voltage difference and rectification characteristics of asymmetric nanopores

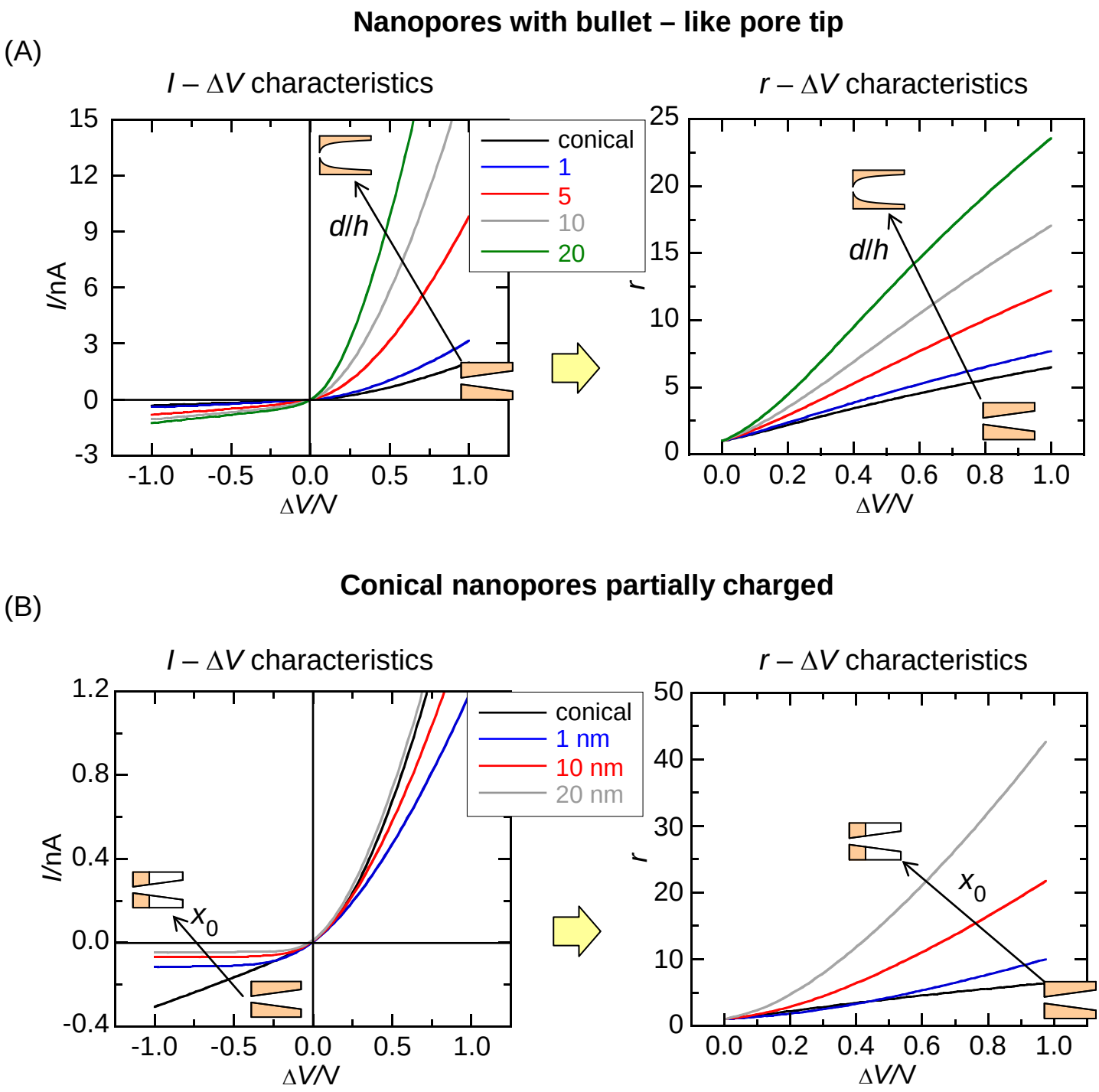

Figure 2

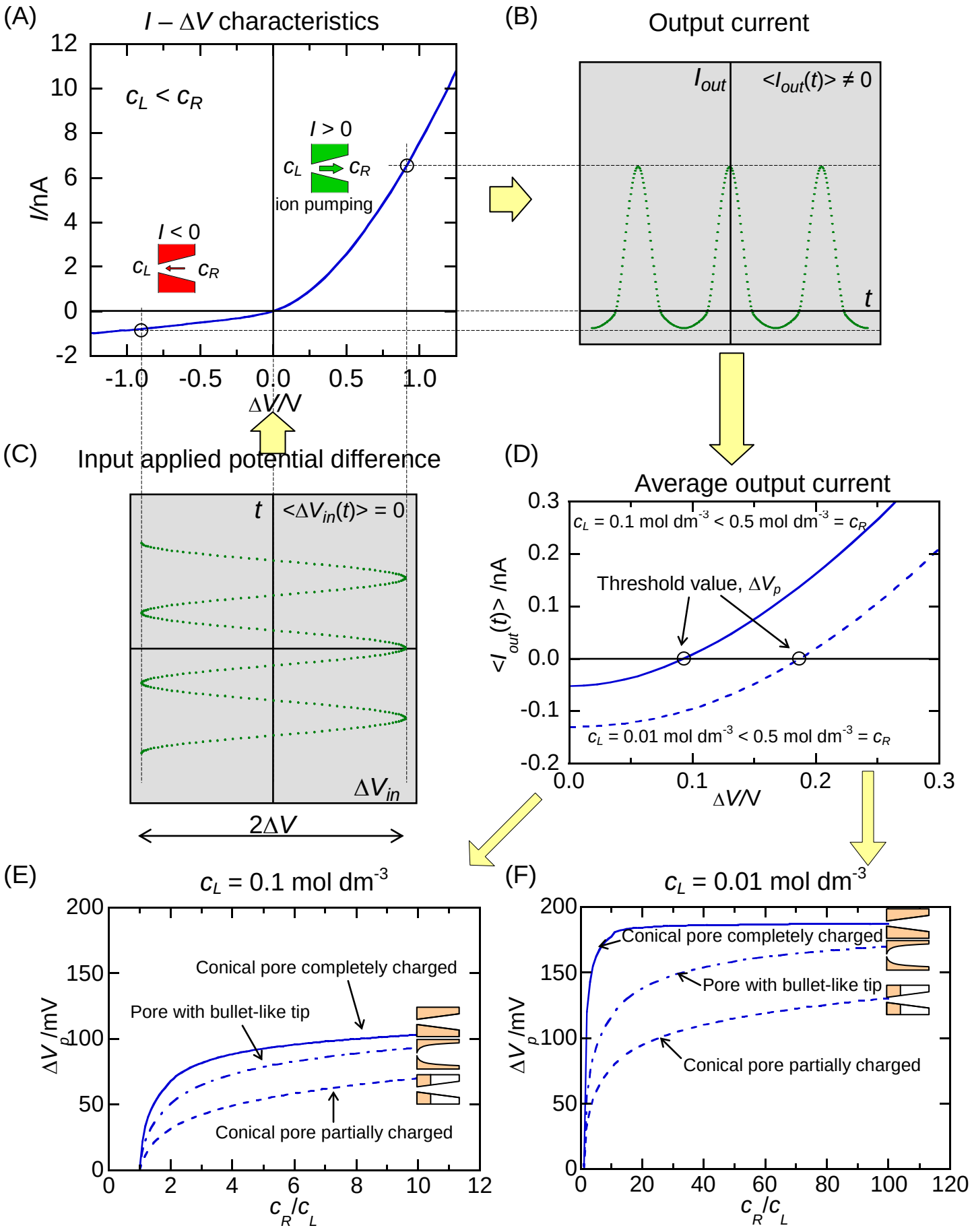
(A)
I – ΔV characteristics
I/nA
ΔV/V
c_L < c_R
I > 0
c_L
c_R
ion pumping
I < 0
(B)
Output current
I_out
<I_out(t)> ≠ 0
t
(C)
Input applied potential difference
t
<ΔV_in(t)> = 0
ΔV_in
2ΔV
(D)
Average output current
<I_out(t)> /nA
c_L = 0.1 mol dm^-3 < 0.5 mol dm^-3 = c_R
Threshold value, ΔV_p
c_L = 0.01 mol dm^-3 < 0.5 mol dm^-3 = c_R
(E)
c_L = 0.1 mol dm^-3
ΔV_p /mV
Conical pore completely charged
Pore with bullet-like tip
Conical pore partially charged
c_R/c_L
(F)
c_L = 0.01 mol dm^-3
ΔV_p /mV
Conical pore completely charged
Pore with bullet-like tip
Conical pore partially charged
c_R/c_L

Figure 3

Logic gate using asymmetric nanopores

(A)

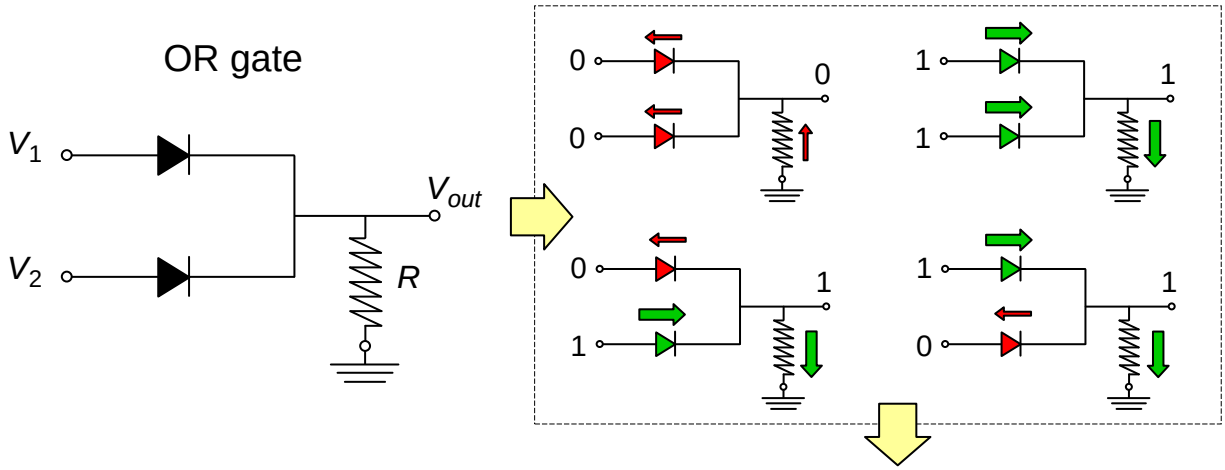

(B)

$I - \Delta V$ characteristics

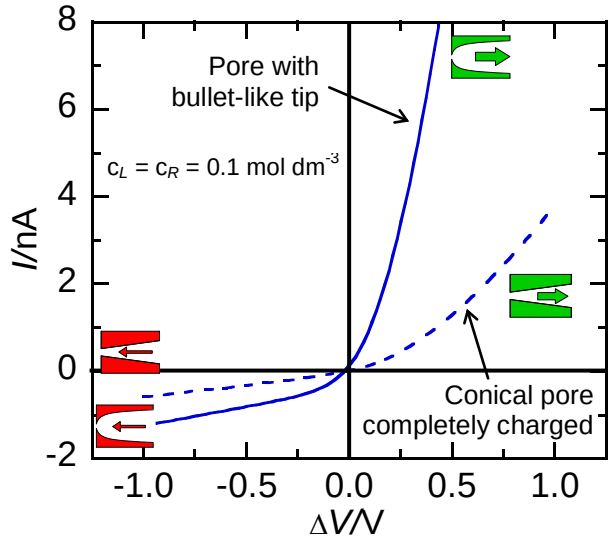

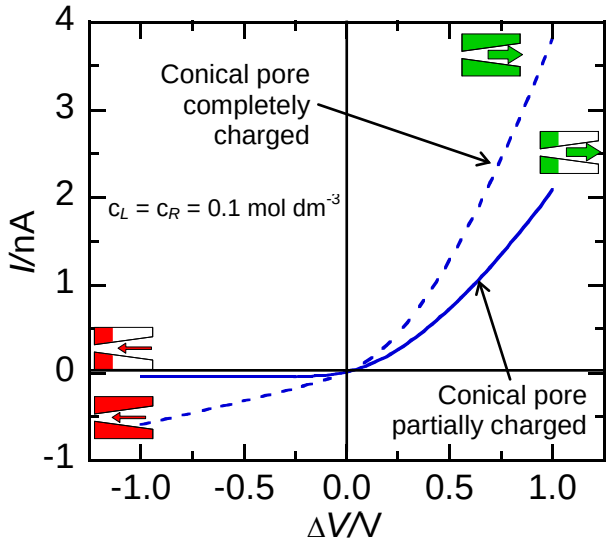

Truth tables

Conical pore completely charged

V_1 /V	V_2 /V	V_{out} /V	$\lvert V_{out}/ V_{out,min}\rvert$
-1 (0)	-1 (0)	-0.11 (0)	1
1 (0)	1 (1)	0.20 (1)	1.8
1 (1)	-1 (0)	0.20 (1)	1.8
1 (1)	1 (1)	0.37 (1)	3.4

Pore with bullet-like tip

V_1 /V	V_2 /V	V_{out} /V	$\lvert V_{out}/ V_{out,min}\rvert$
-1 (0)	-1 (0)	-0.21 (0)	1
1 (0)	1 (1)	0.58 (1)	2.8
1 (1)	-1 (0)	0.58 (1)	2.8
1 (1)	1 (1)	0.73 (1)	3.5

Conical pore partially charged

V_1/V	V_2/V	V_{out} /V	$\lvert V_{out}/ V_{out,min}\rvert$
-1 (0)	-1 (0)	-0.009 (0)	1
1 (0)	1 (1)	0.16 (1)	17.8
1 (1)	-1 (0)	0.16 (1)	17.8
1 (1)	1 (1)	0.26 (1)	28.9

Figure 4

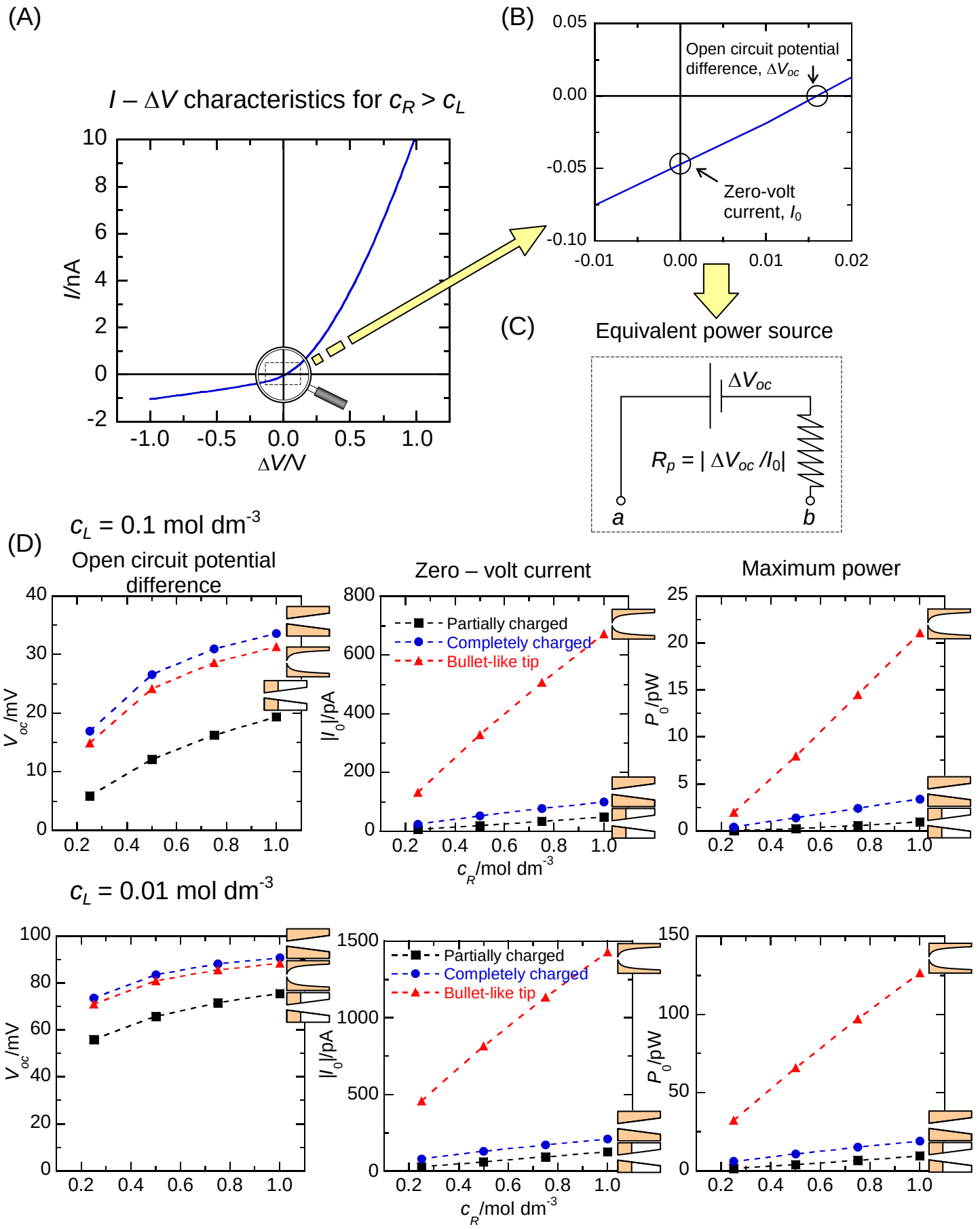
(A)
I – ΔV characteristics for $c_R > c_L$
I/nA
ΔV/V
(B)
Open circuit potential difference, ΔV_{oc}
Zero-volt current, I_0
(C)
Equivalent power source
ΔV_{oc}
$R_p = |\Delta V_{oc}/I_0|$
a
b
(D)
c_L = 0.1 mol dm^{-3}
Open circuit potential difference
Zero – volt current
Maximum power
V_{oc} /mV
$|I_0|$/pA
P_0/pW
Partially charged
Completely charged
Bullet-like tip
c_R/mol dm^{-3}
c_L = 0.01 mol dm^{-3}

Figure 5